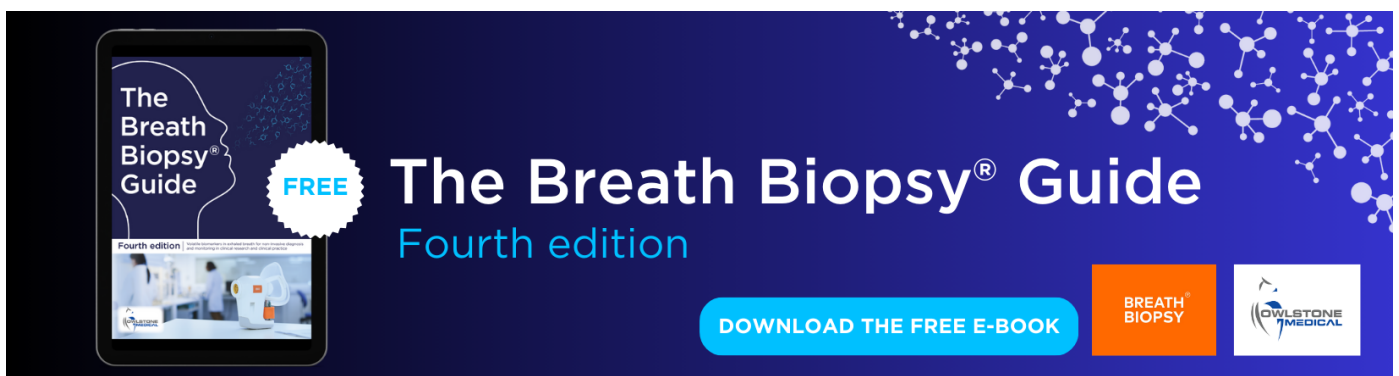**LETTER • OPEN ACCESS**

Predicting compound coastal inundation in 2100 by considering the joint probabilities of landfalling tropical cyclones and sea-level rise

To cite this article: Y Peter Sheng *et al* 2022 *Environ. Res. Lett.* **17** 044055

View the article online for updates and enhancements.

ENVIRONMENTAL RESEARCH
LETTERS

CrossMark

LETTER

Predicting compound coastal inundation in 2100 by considering the joint probabilities of landfalling tropical cyclones and sea-level rise

Y Peter Sheng[*] , Kun Yang and Vladimir A Paramygin

Coastal and Oceanographic Engineering Program, Engineering School of Sustainable Infrastructure and Environment, University of Florida, Gainesville, FL 32611-6580, United States of America
[*] Author to whom any correspondence should be addressed.

E-mail: pete@coastal.ufl.edu

Abstract

In the twenty-first century, the effects of sea-level rise (SLR) and more intense tropical cyclones (TCs) are increasing compound coastal inundation worldwide. To facilitate the adaptation efforts being made by coastal communities, here, we use a coastal surge-wave model together with a novel statistical approach to incorporate the six joint probability density functions (PDFs) of five landfall TC parameters and SLR values, instead of the traditional five-parameter approach, which considers the five PDFs of TCs with prescribed SLR values as boundary conditions. The five-parameter approach determines the 1% annual chance of coastal inundation by conducting numerous sets of surge-wave simulations, each for a different SLR scenario, for the future TC ensemble. The six-parameter approach, however, uses a future TC and SLR ensemble to conduct only one set of surge-wave simulations without the subjective selection of an SLR scenario, and is much less uncertain and much more efficient. In this paper, we focus on the 1% risk of inundation in a large coastal flood plain in southwest Florida by incorporating intensifying TCs and accelerating SLR under a representative concentration pathway 8.5 climate scenario in 2100. The 1% risk of inundation determined by the six-parameter approach is comparable to that obtained from the traditional approach forced with the *expected* SLR value in 2100. The total inundation volume, total inundation area, average inundation height, and maximum inundation height are expected to dramatically increase by (5.7, 2.4, 2.6, and 2.5) times, respectively, compared to their 1982–2009 values. The coastal inundations caused by TCs and SLR are found to interact nonlinearly over the coastal flood plain. Near the coast, TCs account for 70%–80% of the total 1% inundation risk for 1 m of SLR and 30%–70% for 2 m of SLR. Therefore, future inundation analyses must consider TCs and their nonlinear interaction with SLR-induced inundation. These findings will inform local communities and help them to develop coastal adaptation plans.

1. Introduction

Coastal flood vulnerability has been significantly increasing all over the world due to a gradually accelerating sea-level rise (SLR) [1–3], intensifying tropical cyclones (TCs) [4–6], and changing exposure [7, 8]. The SLR accompanying the current warming will lead to higher storm inundation and sea level, assuming that all other factors are unchanged [6]. Future TCs, particularly those in the North Atlantic basin, have been predicted by most climate models to become more intense in the twenty-first century [4–6]. Coastal communities have experienced a dramatic increase in TC-induced flood damage [7], which is highly dependent on the local conditions, including floods, waves, infrastructure, SLR, the landscape, and their interactions [8]. To minimize future flood damage, regional- and local-scale adaptation plans need to be developed based on our best understanding of how intensifying TCs and accelerating

SLR will impact local coastal flood vulnerability in the twenty-first century. The status quo probabilistic coastal flood analysis framework [9] needs to be improved to incorporate the impacts of future TCs and SLR in a changing climate.

Despite a few studies of future storm surges at coastal stations [10–12] over a continental scale due to TCs and SLR, studies of future flood hazards in large coastal floodplains (which are needed for coastal management and infrastructure decisions) are scarce. A recent study [13] simulated the effect of two SLR scenarios during two hypothetical TCs on coastal flooding in Jamaica Bay, NY, while others [14, 15] have studied the increase in flood frequency due to SLR, assuming that there will be no significant changes in storminess. Condon and Sheng [16] used a coastal surge-wave model and the joint probability method with optimal sampling (JPM-OS) to simulate the 2100 coastal flooding in southwest Florida (SWFL), incorporating SLR and TCs with increasing intensity but decreasing frequency. The JPM-OS considered the five-parameter (5P) joint probabilities of the five characteristics of landfalling TCs to simulate probabilistic coastal flooding using specified SLR values (with different probabilities) at the open boundary of the coastal model.

While regional- and local-scale probabilistic coastal flood maps for the twenty-first century are needed for adaptation planning and infrastructure management, there are several major challenges. First, there are considerable uncertainties in the prediction of future TCs by climate models and downscaling models [4, 6, 7], which is also the case for the prediction of future SLR [1–3]. A comprehensive uncertainty analysis of future TC predictions, however, requires extensive data from many models and is beyond the scope of this paper. Here, we focus on the statistical method of integrating the probability density functions (PDFs) of TCs and SLR, instead of a sensitivity study on the effect of coastal inundation vulnerability to climate and downscaling models.

We consider the TCs predicted by the Florida State University global spectral model (FSUGSM) [17, 18], a global atmospheric model (based on the sea surface temperature (SST) and fluxes predicted by the CAMESM2 [19] global climate model for representative concentration pathway 8.5 (RCP8.5) [20, 21] in 2100) downscaled by a 12 km resolution regional climate model weather research forecast (WRF) [22]. To estimate the impact of climate change due to global warming, the RCPs, which consist of a set of greenhouse gas concentration pathways, have been used for climate predictions. RCP 8.5 assumes that greenhouse gas emissions will continue to rise throughout the twenty-first century and that the radiative forcing value in the year 2100 will be $+8.5$ W m^{-2} relative to the pre-industrial value [20, 21]. While the accuracy of the TCs predicted by FSUGSM-WRF for 2100 is uncertain, TCs predicted by the FSUGSM-WRF for

the period from 1990–2010 were found to produce a 1% risk of coastal inundation in SWFL, which is similar to that determined using historical TC data in 1982–2009 [23]. The SLR under RCP8.5 could reach as much as 2 m by 2100[2]. However, it should be noted that the SLR could exceed 2 m if marine ice-cliff instability processes are included in the projections, but these high-end sea-level rise projections cannot provide an unambiguous probability distribution [24]. PDFs of the global mean sea level (GMSL) and the regional/local sea level (RSL) at Naples, Florida, in 2100 were provided by Jevrejeva *et al* [25] and Kopp *et al* [1], respectively. The projections from Kopp *et al* [1] include estimates for the expected contributions to the relative sea-level rise from vertical land motion for specific tidal gauge locations. The vertical land motion contribution varies spatially, and therefore projections differ for the Fort Myers and Naples tidal gauges in the study area, but the difference is very small, and the Naples tidal gauge data is representative of the SWFL.

Another major challenge is the additional uncertainty and prohibitive computational requirements associated with the status quo 5P JPM-OS for TCs and selected SLR scenarios. Coastal surge and wave simulations for each TC ensemble must be conducted for many SLR values (with different probabilities). Here, we present a novel statistical method to reduce the uncertainty and computational effort of assessing probabilistic coastal flooding in the twenty-first century by incorporating the six-parameter (6P) joint probabilities of TC characteristics and SLR. We focus on a large coastal flood plain in SWFL (figure 1) which is highly vulnerable to coastal flooding due to a high SLR projection, frequent TCs, a low elevation with flat coastal bathymetry and topography, and growing population and development. While the uncertainties associated with coastal surge-wave models have been addressed elsewhere [9, 26], we will compare the probabilistic coastal floods simulated by two coastal models, CH3D (**C**urvilinear-grid **H**ydrodynamics in **3D**)-SWAN **S**imulating **WA**ves **N**earshore) [27–31] and SLOSH (**S**ea, **L**ake, and **O**verland **S**urge from **H**urricanes) [31], which have different model physics and grid resolutions.

2. Results

2.1. Probabilistic coastal inundation maps for the current climate and 2100 under RCP8.5

Using CH3D-SWAN and JPM-OS, we developed probabilistic coastal inundation maps for the current climate (1982–2009) [23] and 2080–2100 under RCP8.5 based on the TCs predicted by the FSUGSM-WRF. The probabilistic coastal inundation maps for 2080–2100 were developed in three different ways: (a) 5P JPM-OS, using the PDFs of the five TC characteristics and the expected value of the GMSL specified at the open boundary of the coastal model domain;
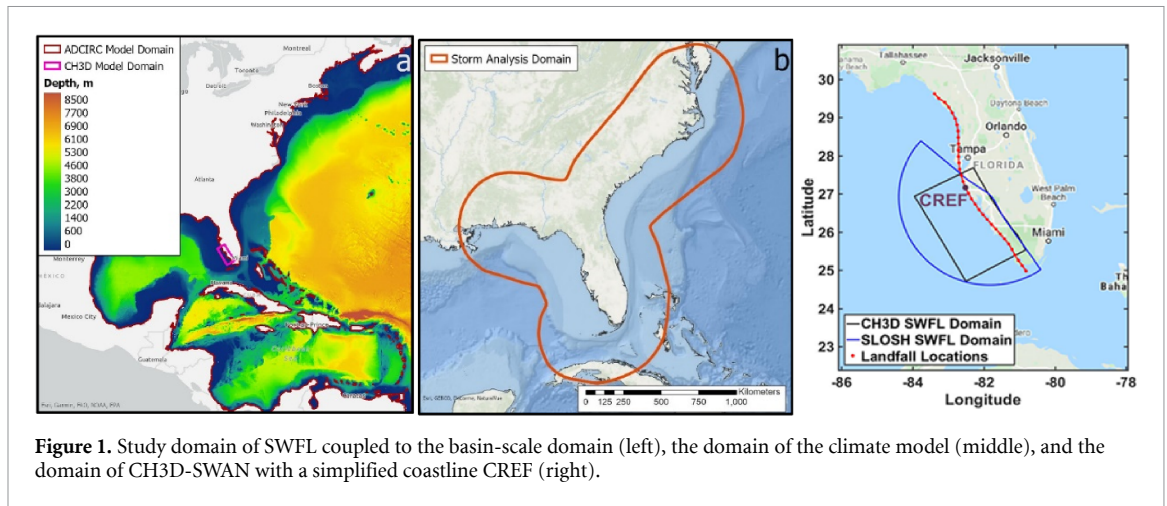
Figure 1. Study domain of SWFL coupled to the basin-scale domain (left), the domain of the climate model (middle), and the domain of CH3D-SWAN with a simplified coastline CREF (right).

(b) 6P JPM-OS, using the six PDFs of the five TC characteristics and the GMSL; and (c) 6P JPM-OS, using the six PDFs of the five TC characteristics and the RSL at Naples tide station.

2.2. 1% annual chance coastal inundation maps developed using 5P JPM-OS for the current climate

The 1% annual chance coastal inundation map shown in figure 2(a) was developed using CH3D-SWAN and 5P JPM-OS with historical TC data for 1982–2009. The PDFs of five TC characteristics (P_c, R_m, V_f, θ, L_0), i.e. (the central pressure deficit, the radius of maximum wind, the forward speed, heading, and landfall location) were considered in the selection of the optimal TCs. While the maximum 1% inundation reached more than 2 m, there is significant spatial variation in the inundation height over the coastal flood domain. The 1% annual chance flood elevation at the Naples tide station compares well with that determined from the historical water-level data at Naples using the peak over threshold (POT) method [11]. The inundation area and inundation height agree well with the 1% annual chance still-water elevation for the region developed by the Federal Emergency Management Agency.

2.3. 1% annual chance inundation maps obtained using 5P JPM-OS and the expected GMSL for 2100

JPM and JPM-OS were used with the PDFs of (P_c, R_m, V_f, θ, L_0) of TCs predicted by FSUGSM-WRF for 2100 under the RCP8.5 scenario, while the expected value of the GMSL (0.9 m, see section 4) was specified at the open boundary of the coastal model domain. The 5P JPM considers an ensemble of 20 625 TCs, out of which, 150 optimal TCs were selected by 5P JPM-OS, following the optimal TC selection method [23]. The 1% inundation maps produced by JPM-OS and a prescribed SLR of 0.9 m with CH3D-SWAN are shown in figure 2(b). Both the inundation height and the total inundation area (TIA) are more than doubled compared to the current climate values shown in figure 2(a).
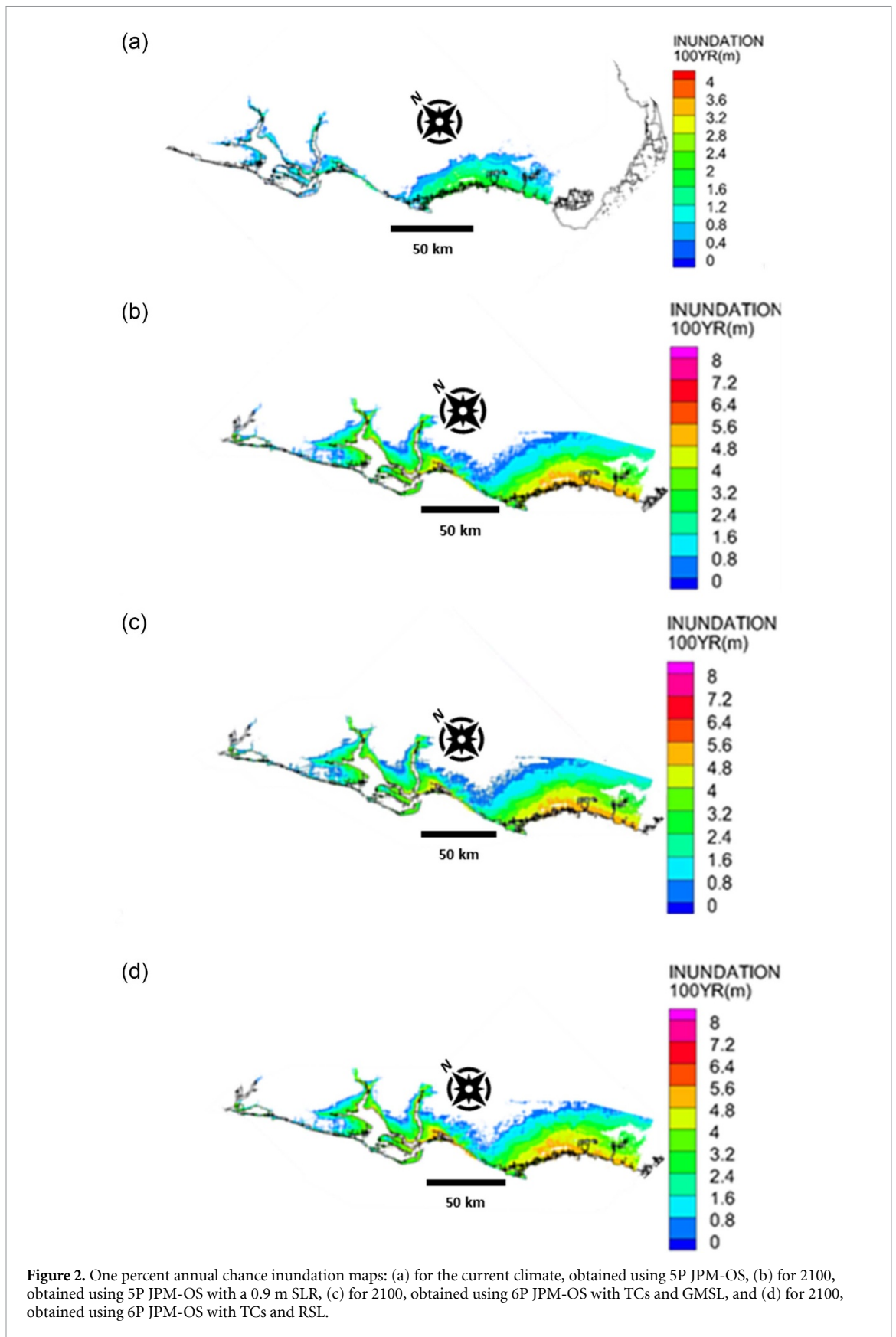
2.4. 1% annual chance inundation maps obtained using 6P JPM-OS and the GMSL for 2100

The 1% annual chance coastal inundation map developed with 6P JPM-OS using the PDFs of (P_c, R_m, V_f, θ, L_0, GMSL) for 2100 under the RCP8.5 scenario is shown in figure 2(c). The map was produced using the CH3D-SWAN results for 350 optimal TC&SLR combinations instead of the full JPM ensemble of 103 125 TC and SLR combinations. SLOSH was found to overestimate the coastal inundation due to its simpler physics and lower resolution. However, the highly efficient SLOSH was used solely to determine the optimal TC&SLR combinations for the 6P JPM-OS to save computational time. The optimal TCs determined by SLOSH were found to be very similar to those determined by the CH3D-SWAN in the 5P JPM-OS [23]. Although we could not verify the agreement between the CH3D-SWAN results obtained by 6P JPM and 6P JPM-OS, inundation maps produced by the 6P JPM-SLOSH and the 6P JPM-OS-SLOSH agreed extremely well, with a coefficient of determination (R^2) of 0.99 and a root mean square error (RMSE) of 0.16 m.

Coastal inundation maps produced using the expected GMSL value of 0.9 m with 5P JPM and JPM-OS (figure 2(b)) are very similar to those produced with the 6P JPM and JPM-OS (figure 2(c)). This is because the nonlinear effect of SLR on storm surge is comparable for different levels of SLR [32, 33].

2.5. 1% annual chance inundation maps obtained using 6P JPM-OS with RSL

The 1% annual chance coastal inundation map developed with 6P JPM-OS using the PDFs of (P_c, R_m, V_f, θ, L_0, RSL) for 2100 under the RCP8.5 scenario is shown in figure 2(d). The inundation is very similar to that shown in figure 2(c), because the GMSL is very similar to the RSL at Naples. However, in other places, such as New Jersey and New York [1, 34], the GMSL and RSL can be significantly different; hence, the RSL should be used to develop future coastal inundation maps.

Figure 2. One percent annual chance inundation maps: (a) for the current climate, obtained using 5P JPM-OS, (b) for 2100, obtained using 5P JPM-OS with a 0.9 m SLR, (c) for 2100, obtained using 6P JPM-OS with TCs and GMSL, and (d) for 2100, obtained using 6P JPM-OS with TCs and RSL.

2.6. Comparison of 1% inundation metrics for four scenarios

Table 1 shows a comparison of the 1% inundation risks obtained using the four different scenarios in terms of the 1% inundation metrics: total inundation volume (TIV), TIA, average inundation height (AIH), and maximum inundation height (MIH). TIA and TIV are defined as follows [35]:

Table 1. One percent inundation statistics for the maps shown in figure 1. TIV = total inundation volume, TIA = total inundation area, AIH = average inundation height, MIH = maximum inundation height.

Year	Scenario	TIV (10^9 m^3)	TIA (10^9 m^2)	AIH (m)	MIH (m)
1892–2009	5P JPM-OS with TC	2.8	2.6	1.1	2.4
2080–2100	5P JPM-OS with TC & E(GMSL)	15.4	5.8	2.8	6.1
2080–2100	6P JPM-OS with TC & GMSL	16.0	6.1	2.8	6.2
2080–2100	6P JPM-OS with TC & RSL	15.1	6.1	2.7	6.1

$$\text{TIA} = \int\int_{\text{Landward Area}} dx dy \tag{1}$$

$$\text{TIV} = \int\int_{\text{Landward Area}} [H_{\max}(x,y) - H_0(x,y)] dx dy \tag{2}$$

where $H_{\max}(x,y)$ and $H_0(x,y)$ are the maximum water level and the land elevation at the land cell (x,y), respectively, for each scenario. MIH = maximum inundation height, while the AIH is the average value of the MIH over the entire domain. These statistics have been used as objective metrics to quantify the TC-induced flood hazard over a coastal flood plain by a single TC as well as the 1% flood due to a TC ensemble [35–37].

While the coastal inundation maps for 2080–2100 shown in figures 2(b)–(d) and the inundation metrics (table 1) agree very well, the inundation metrics for 2080–2100 are dramatically higher than those for the current climate (1982–2009), which agree well with those for the period of 1990–2010 [23]. The 2080–2100 inundation metrics are alarmingly (5.7, 2.4, 2.6, and 2.5) times those for the period 1982–2009 for (TIV, TIA, AIH, and MIH) respectively. These results contain uncertainties associated with the prediction of future TCs by climate and downscaling models, coastal model simulation, the statistical method, as well as other factors that are neglected in this analysis (e.g. precipitation and changing land use features over time, etc). A comprehensive study to address these uncertainties is needed but is beyond the scope of this study. Further discussion will be provided in the next section of this paper.

The simulated inundation metrics (TIV, TIA, AIH, and MIH) for 2080–2100 under the RCP4.5 scenario with 1 m of SLR determined by the FSUGSM-WRF and the GFDL6-KE [7, 36] are (2.71, 1.84, 1.88, and 3.45) times and (2.14, 1.44, 1.68, and 3.40) times the corresponding values for the current climate, respectively.

2.7. Relative importance of TCs and SLR for coastal inundation
Here, we examine the relative importance of TCs and SLR in term of their effects on the 1% coastal flood hazard. We consider three simulations obtained using the TCs predicted by FSUGSM-WRF for 2100 under

the RCP4.5 scenario with three SLR values: 0, 1, and 2 m. We then subtract the inundation obtained for SLRs of 1 and 2 m (H_{withSLR}) from that obtained without SLR (H_{noSLR}) and obtain the percentage of inundation due to SLR (P_c) and the percentage of increased inundation as a fraction of the SLR (P_i):

$$P_c = \frac{H_{\text{withSLR}} - H_{\text{noSLR}}}{H_{\text{withSLR}}} \tag{3}$$

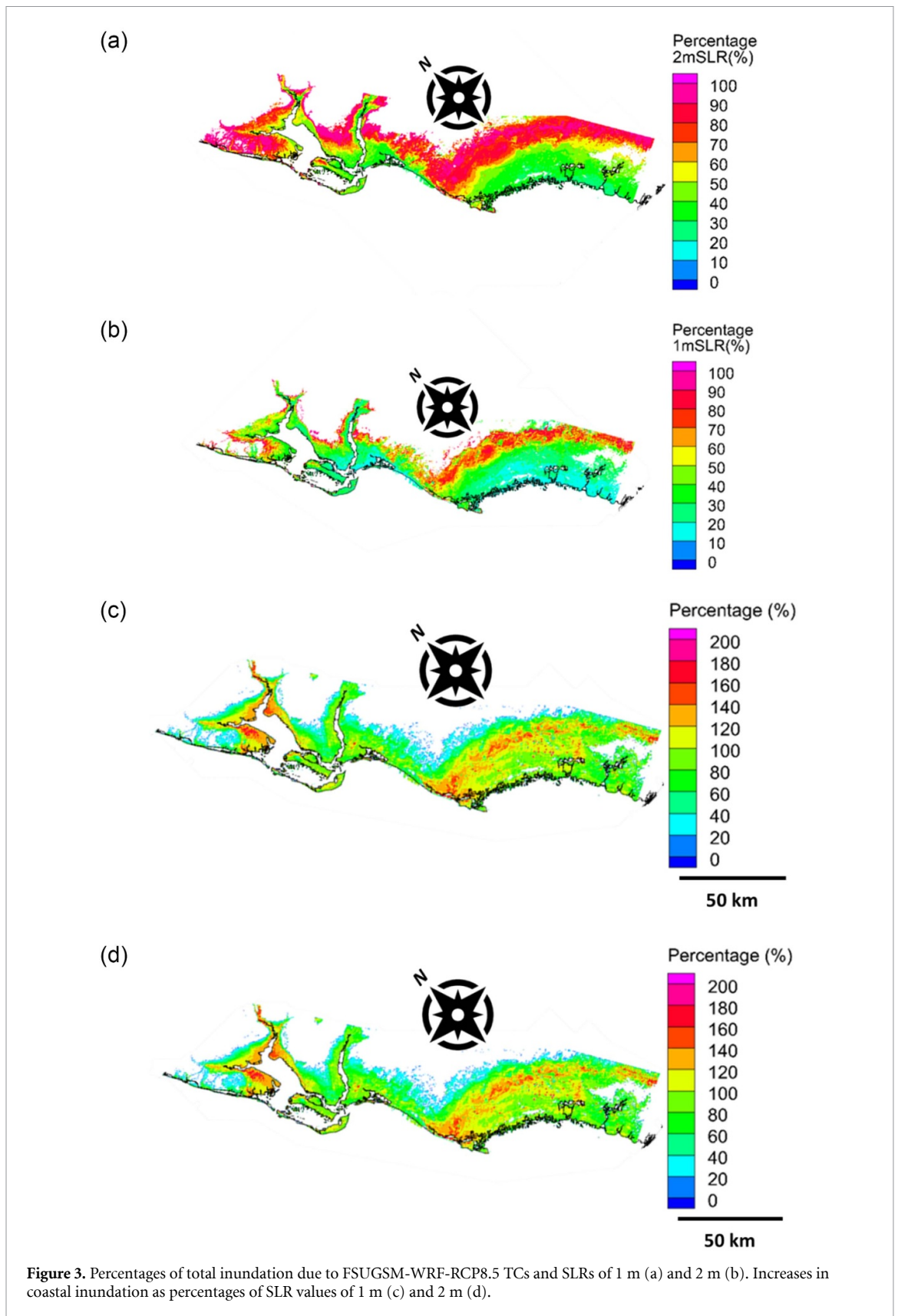$$P_i = \frac{H_{\text{withSLR}} - H_{\text{noSLR}}}{\text{SLR}}. \tag{4}$$

As shown in figures 3(a) and (b), SLR plays a dominant role at the inland boundary. Near the coast, storm surge due to TCs accounts for 70%–80% of the total inundation (for a 1 m SLR) or 30%–70% (for a 2 m SLR). Therefore, TCs cannot be ignored in the development of future coastal flood maps. Figures 3(c) and (d) indicate that the effect of SLR on inundation varies significantly over the floodplain, due to nonlinear interactions between storm surge and SLR. Near the shoreline of Rookery Bay and Charlotte Harbor, inundation is increased by 1.6 m due to a 1 m SLR. This shows that SLR-induced coastal inundation can be significantly amplified or reduced by the surge–SLR interaction, depending on location. Hence, coastal flood maps produced by the simple addition of an SLR value to historical estimates of the 1% inundation level are highly inaccurate!

3. Discussion

3.1. Uncertainties of future inundation prediction
While a few studies have assessed the impact of SLR and TCs predicted by a few climate models and one downscaling model on future storm surges and waves in open-water stations over the continental scale [10, 11], no study has predicted detailed inundation over a large coastal flood plain using the joint probabilities of a large TC ensemble and SLR.

Predictions of future probabilistic coastal inundation contain uncertainties from numerous sources, including the predictions of future TCs (which depend on climate models, downscaling models, and RCP scenarios), SLR, coastal surge and wave models, hurricane wind models, precipitation, statistical methods. A comprehensive assessment of all the uncertainties is a gigantic task beyond the scope of this paper. A future study will address the sensitivity

Figure 3. Percentages of total inundation due to FSUGSM-WRF-RCP8.5 TCs and SLRs of 1 m (a) and 2 m (b). Increases in coastal inundation as percentages of SLR values of 1 m (c) and 2 m (d).

of future probabilistic coastal inundation to predicted future TCs by all coupled model intercomparison project phase 5 (CMIP5) [38] and coupled model intercomparison project phase 6 (CMIP6) [39] climate models and numerous downscaling models

[7, 22, 39, 40]. Although the detailed results are not presented here, we found the probabilistic coastal inundation in SWFL due to TCs predicted by FSUGSM-WRF and GFDL6-KE [7, 36] (GFDL6 predicted TCs downloaded by Emanuel's deterministic

statistical model) for RCP4.5 in 2100 to be quite comparable.

3.2. Uncertainty and efficiency of the statistical method

Here, we address the uncertainty associated with the JPM and JPM-OS statistical methods and compare the results obtained by two coastal models, CH3D-SWAN and SLOSH. A study [25] compared the performance of five storm surge modeling systems, including CH3D-SWAN and SLOSH, used to simulate coastal flooding during a single TC as well as 1% coastal flooding in SWFL.

The uncertainties of probabilistic coastal flooding have been studied from different perspectives. A study [41] provided a comprehensive review of the aleatory and epistemic uncertainties of JPM and JPM-OS for TCs and showed the epistemic uncertainty along one transect. Another [41] discussed the return period of Superstorm Sandy under a future climate with a 90% confidence interval, with a focus on storm surges at coastal tidal gauges rather than inundation over a large coastal flood plain. Yang *et al* [37] applied JPM-OS with kriging interpolation in a rapid forecasting and mapping system for the Florida Gulf coast and estimated the uncertainty of the forecasted water levels during individual TCs. In the following, we assess the uncertainty associated with the 6P JPM and JPM-OS used to develop the 1% inundation maps for 2100 with a 95% confidence interval.

The root mean-square error (RMSE) of the kriging interpolation can be directly estimated along with the interpolated water level [23]. The annual rate of occurrence of a water level greater than a specific value η with a 95% confidence interval for a grid cell inside the domain is calculated by:

$$
\begin{aligned}
P[\eta_+ > \eta] &= \lambda \int \ldots \int^{\boldsymbol{x}} f_X(\boldsymbol{x}) P[\eta(\boldsymbol{x}) \\
&\quad + 1.96 * \mathrm{RMSE}(\boldsymbol{x}) > \eta]\, \mathrm{d}\boldsymbol{x} \\
&\approx \sum_{i=1}^{n} \lambda_i P[\eta(\boldsymbol{x}_i) + 1.96 * \mathrm{RMSE}(x) > \eta]
\end{aligned}
\tag{5}
$$

$$
\begin{aligned}
P[\eta_- > \eta] &= \lambda \int \ldots \int^{\boldsymbol{x}} f_X(\boldsymbol{x}) P[\eta(\boldsymbol{x}) \\
&\quad - 1.96 * \mathrm{RMSE}(\boldsymbol{x}) > \eta]\, \mathrm{d}\boldsymbol{x} \\
&\approx \sum_{i=1}^{n} \lambda_i P[\eta(\boldsymbol{x}_i) - 1.96 * \mathrm{RMSE}(x) > \eta]
\end{aligned}
\tag{6}
$$

where $\mathrm{RMSE}(\boldsymbol{x})$ is the RMSE of the interpolated water level of the test $\mathrm{TC}(\boldsymbol{x})$, and η_+ and η_- are the upper and lower limits of the annual rate of occurrence of the water level with a 95% confidence interval. The upper and lower uncertainties δ_+ and δ_- can be calculated as follows:

$$
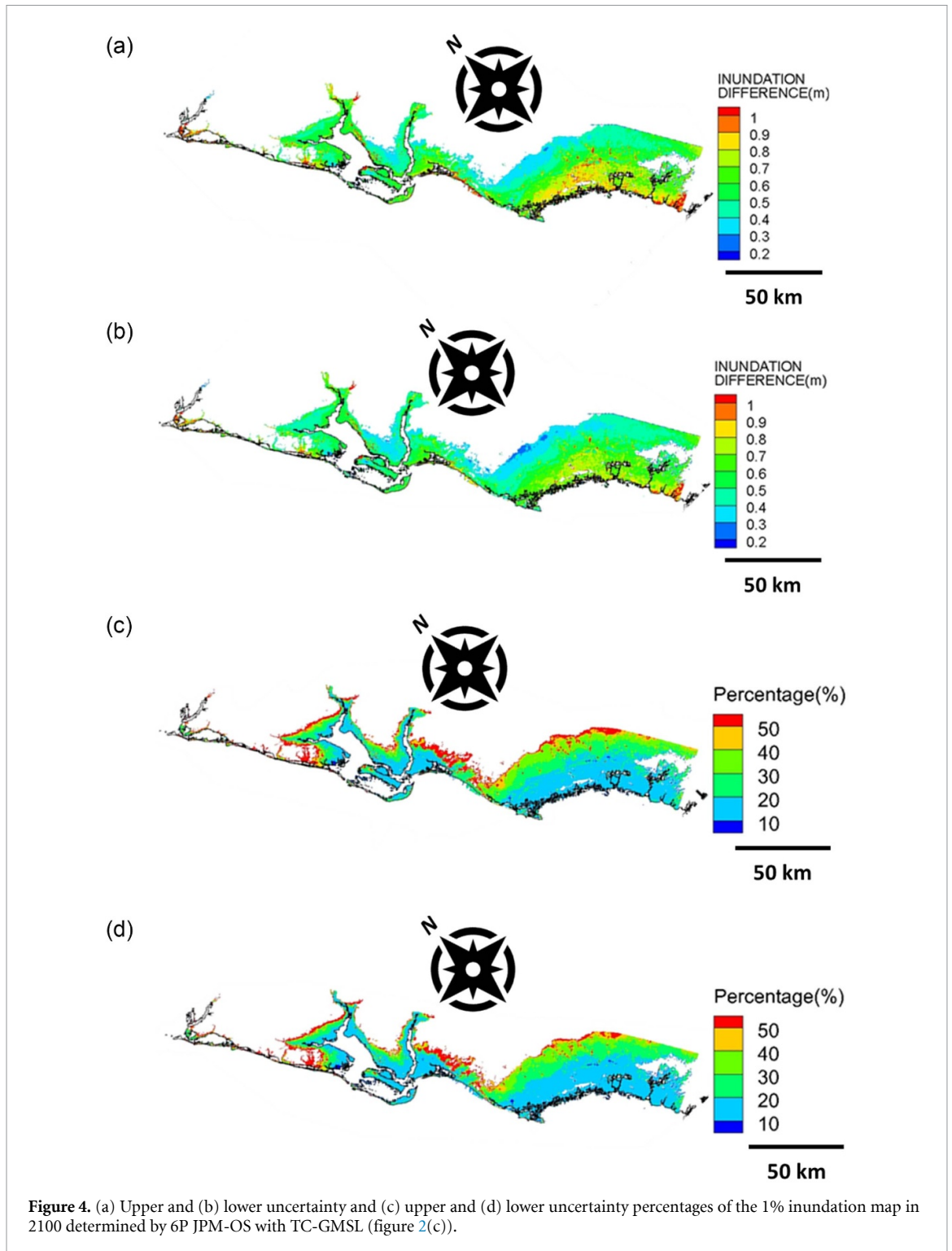\delta_+ = \eta_+ - \eta_0
\tag{7}
$$

$$
\delta_- = \eta_0 - \eta_-
\tag{8}
$$

where η_0 is the annual rate of occurrence of the water level without any uncertainty. The upper and lower uncertainties are then divided by η_0 to calculate the upper and lower uncertainty percentages P_+ and P_-. Figures 4 and 5 show the upper and lower uncertainties and uncertainty percentages of the 1% inundation maps obtained using 6P JPM-OS and 5P JPM-OS with expected GMSL value, $E(\mathrm{GMSL})$, respectively. For the 6P case, the upper and lower uncertainties are within 1 m in the nearshore area and decrease further inland. The upper and lower uncertainty percentages are less than 20% in the nearshore area and increase to 50% further inland. For the 5P case, the upper uncertainty reaches 2 m at some nearshore location, which is higher than the lower uncertainty. Both the uncertainty and the uncertainty percentage obtained from 6P JPM-OS are much lower than those obtained from 5P JPM-OS, mainly because 6P JPM-OS selects and utilizes more optimal TCs, compared to 5P JPM-OS. These account for the uncertainties of kriging interpolation, but not the uncertainties of other factors, such as storm surge models [9, 26], the Holland wind model [42], the CMIP5 [38] and CMIP6 [43] climate models, various downscaling models [7, 22, 39, 40], etc.

Figures 4 and 5 clearly show that the 6P JPM-OS with the TC and SLR ensemble contains much less uncertainty than the 5P JPM-OS with the prescribed expected GMSL value, and hence should be the preferred method for developing probabilistic coastal flood maps. Moreover, the normalized computational time and disk space required to produce high-resolution inundation maps using 6P JPM-OS are much smaller than those of the other methods, as shown in SI-1 (available online at stacks.iop.org/ERL/17/044055/mmedia).

3.3. CH3D-SWAN vs SLOSH results

Due to its very high efficiency, SLOSH was used for the determination of optimal storms in the JPM-OS. The optimal storms were used by both SLOSH and CH3D-SWAN to determine the 1% coastal inundation. The 1% coastal inundations determined by SLOSH with JPM and JPM-OS are comparable. However, the SLOSH results show much higher inundation than the CH3D-SWAN results, which is primarily due to the coarser grid resolution and partially due to the simpler physics of SLOSH. These results are discussed further in SI-2.
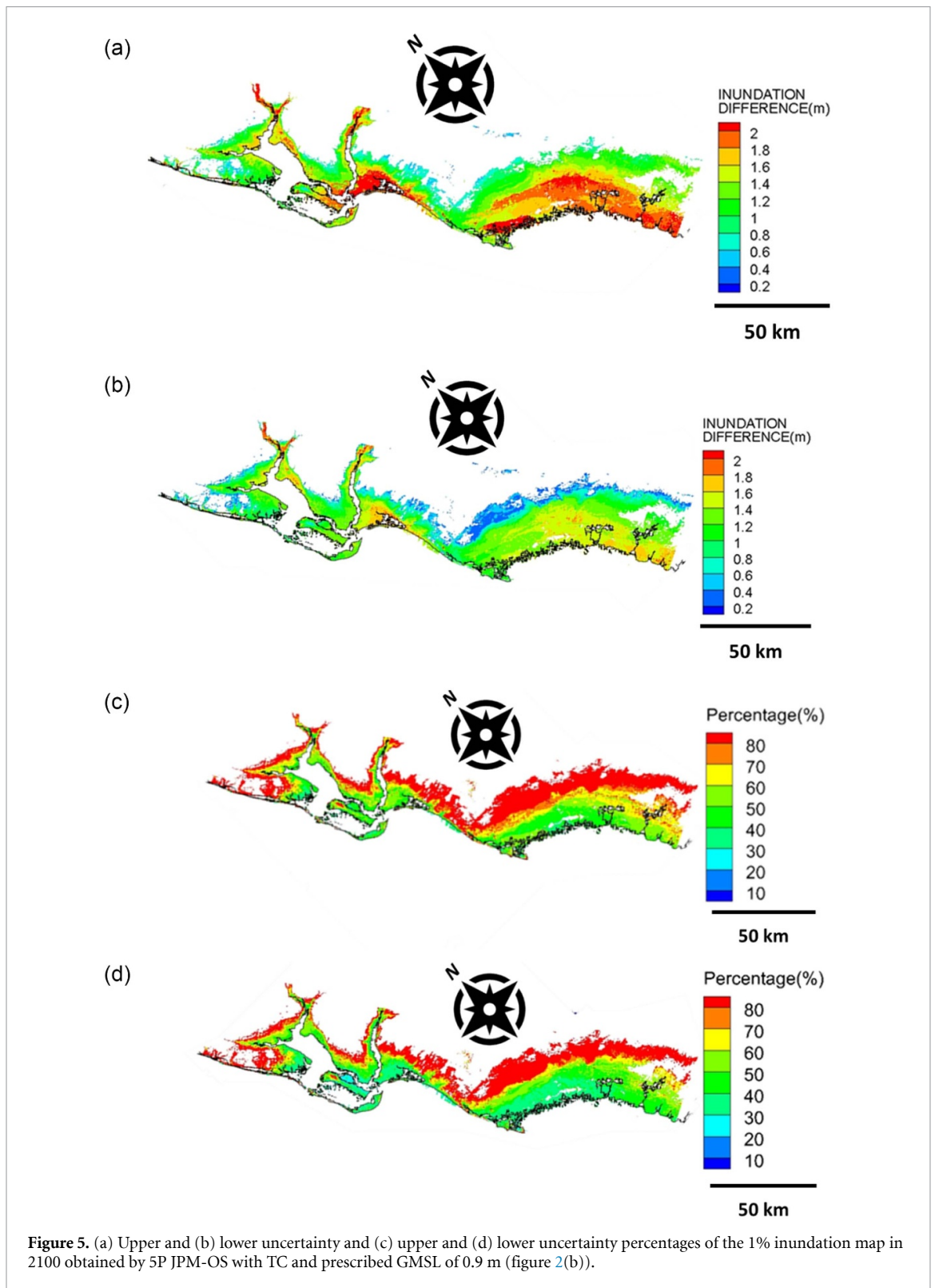
Figure 4. (a) Upper and (b) lower uncertainty and (c) upper and (d) lower uncertainty percentages of the 1% inundation map in 2100 determined by 6P JPM-OS with TC-GMSL (figure 2(c)).

4. Methods

4.1. Coastal surge-wave model

This study uses the coupled coastal surge-wave model CH3D-SWAN [26–30], which has been extensively applied throughout the US Atlantic and Gulf coasts, along with the JPM-OS [23, 36], to simulate future coastal inundation due to the joint probabilities of future TCs and SLR. As shown in figure 1(c), the CH3D-SWAN domain for SWFL has a minimum resolution of ~20 m with an average grid size of ~200 m, while the SLOSH domain has a minimum resolution of ~200 m with an average grid size of ~1500 m. For simplicity, this study uses the vertically averaged version of CH3D [8] instead of the three-parameter version. The ability of CH3D-SWAN to simulate TC-induced coastal inundation in SWFL has been verified for hurricanes Charley [26], Wilma [37], and Irma [37]. For efficiency, SLOSH was used to determine the optimal TCs for JPM-OS, while

Figure 5. (a) Upper and (b) lower uncertainty and (c) upper and (d) lower uncertainty percentages of the 1% inundation map in 2100 obtained by 5P JPM-OS with TC and prescribed GMSL of 0.9 m (figure 2(b)).

CH3D-SWAN was used to produce an accurate probabilistic coastal inundation map. Details of the CH3D model, the SWAN model, and the SLOSH model can be found in numerous papers in the references, particularly in Sheng *et al* [30], Booij *et al* [31], and Jelesnianski *et al* [44], respectively; hence, they will not be repeated here.

4.2. TCs for 1982–2009 and 2080–2100 under RCP8.5

TCs for 1982–2009, 2020–2040, and 2080–2100 were developed using the FSUGSM [17, 18] and downscaled [22] using a 12 km WRF model [37] for the southeastern US region (figure 1(b)). TCs in 2080–2100 under RCP8.5 were predicted by the FUSGSM
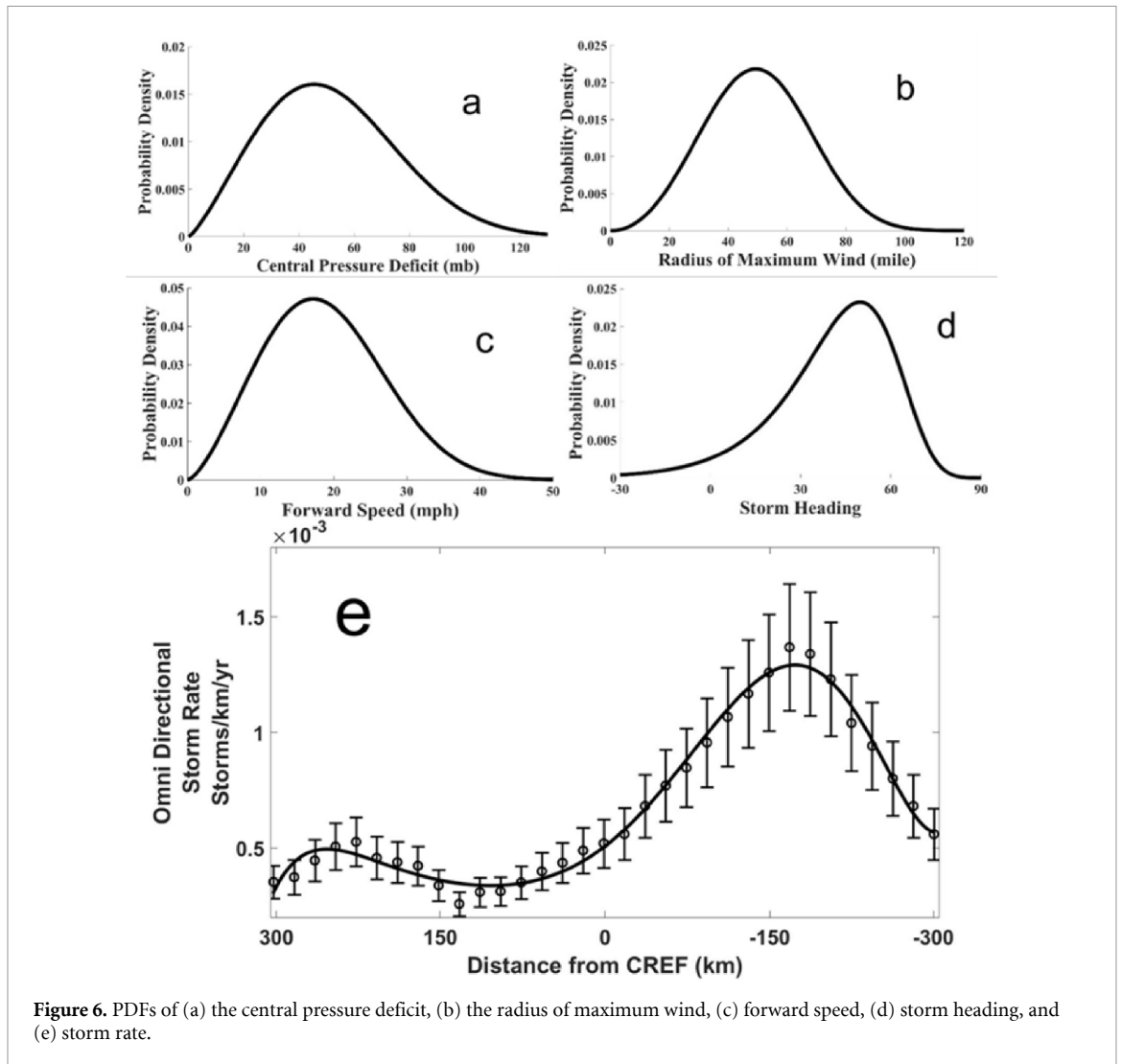
Figure 6. PDFs of (a) the central pressure deficit, (b) the radius of maximum wind, (c) forward speed, (d) storm heading, and (e) storm rate.
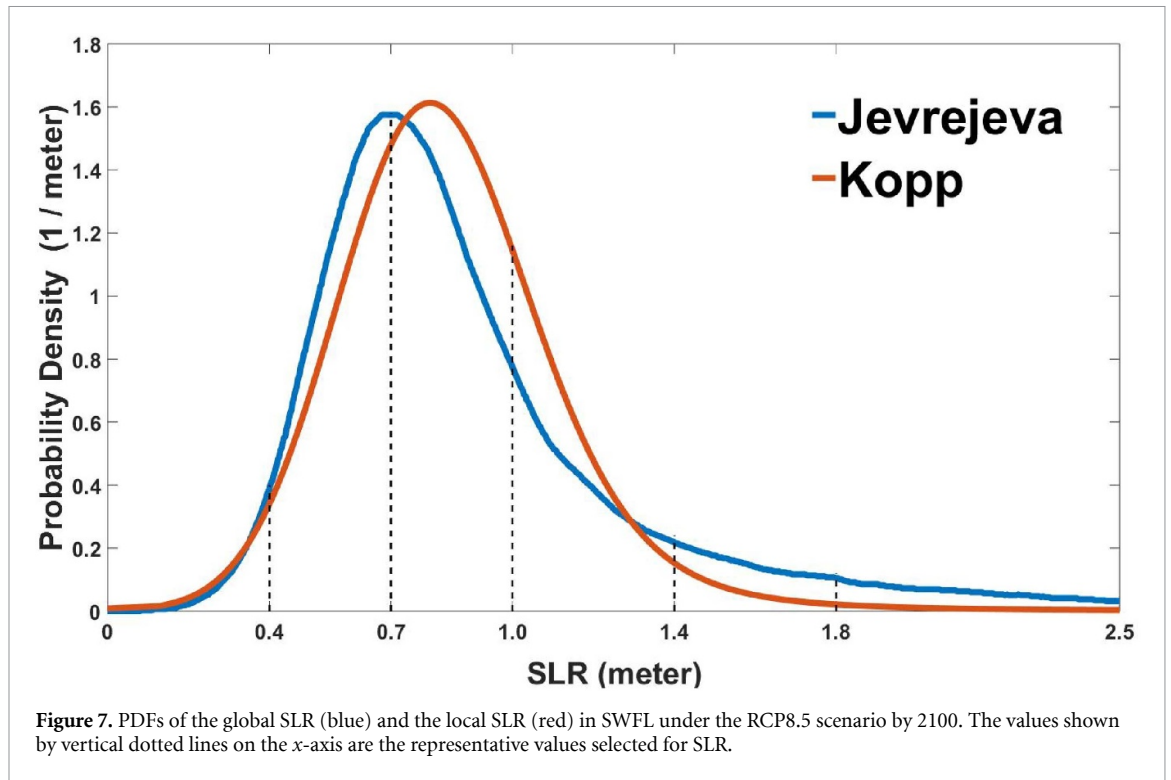
using the predicted SST simulated by the CanESM2 model with a CO_2 concentration of 846 ppm. CanESM2 was found to have the best results for historical SST prediction. The simulation for 1982–2009 resulted in 60 TCs, seven of which made landfall in the SWFL domain (figure 1(c)), which compares well with the 64 historical TCs and seven landfalls during the same period. The 1% flood risks generated based on the simulated and historical TCs compared well [23]. Moreover, the future TCs predicted by the FSUGSM-WRF model cover more climate scenarios in the twenty-first century than any other climate and downscaling model for this region. The 1% coastal flooding risks produced by the TCs predicted by the FSUGSM-WRF model and the GFDL6-KE model for RCP4.5 are comparable. While the TCs predicted by various climate and downscaling models for the current and future climates can be quite different [4, 6], depending on numerous factors (e.g. climate model physics and the TC detection algorithm, climate model resolution, downscaling model method and resolution, etc.), this study focuses on the statistical method used to integrate the PDFs of TCs and SLR, as opposed to a sensitivity study of the effect of coastal

inundation vulnerability to climate and downscaling models. The statistical method presented in this study can readily be applied to TCs developed by any climate model and downscaling model.

The central pressure deficit, radius of maximum wind, storm forward speed, and storm heading direction of landfalling storms in SWFL are calculated, and the best fits of the data to known probability density functions are found using maximum likelihood estimations [16, 23]. The PDFs are shown in figure 6(a)–(d). Storm rates are calculated and fitted to a seventh-order polynomial [45] and plotted in figure 6(e).

4.3. PDF and expected SLR value

The PDFs of SLR (f[SLR]) (figure 7) under the RCP8.5 scenario are based on Jevrejeva *et al* [25] and Kopp *et al* [1] for the GMSL and the RSL at Naples, respectively. Jevrejeva *et al* [25] considered the main sea-level components of thermal expansion, glacier surface mass balance, Greenland surface mass balance and dynamical changes, Antarctica surface mass balance and dynamical changes, and changes in land water storage. They predicted that the probability

Figure 7. PDFs of the global SLR (blue) and the local SLR (red) in SWFL under the RCP8.5 scenario by 2100. The values shown by vertical dotted lines on the *x*-axis are the representative values selected for SLR.

of a GMSL of less than 1.8 m is more than 95%. The expected value of SLR $\{E[\text{SLR}] = \sum \text{slr} * f(\text{slr})\}$, where f is the probability of a specific SLR value, is calculated to be 0.9 m. Kopp *et al* [1] estimated the regional/local sea level (RSL) by considering the changes in ocean dynamics, Earth's gravitational field, glacial isostatic adjustment, and vertical land motion. The PDF is constructed using the 0.5th–99.5th percentile of the predicted local sea level at Naples, FL. The PDF of the RSL is more symmetric and has a lighter tail, compared to that for the GMSL.

4.4. Joint probability method (JPM) and JPM-OS
4.4.1. Joint probability method (JPM)
The traditional 5P JPM considers all possible combinations of five TC parameters and requires the simulation of coastal flooding for an ensemble of TCs called the test TCs $(\boldsymbol{x})$, where $\boldsymbol{x} = [p_c, R_m, \theta, V_f, L_0]$. The new 6P JPM considers all possible combinations of the TC parameters and SLR values and requires the simulation of an ensemble of TCs called the test TCs $(\boldsymbol{x})$, where $\boldsymbol{x} = [p_c, R_m, \theta, V_f, L_0, \text{SLR}]$. The test TCs are simulated by a numerical model to generate the peak water-level height $\eta(x)$. The annual rate of occurrence (such as 1%) of a water level greater than a specific value η for a cell inside the domain is then calculated by:

$$P[\eta_{\max} > \eta] = \lambda \int \ldots \int^{x} f_X(\boldsymbol{x}) P[\eta(\boldsymbol{x}) > \eta] \, \mathrm{d}\boldsymbol{x}$$

$$\approx \sum_{i=1}^{n} \lambda_i P[\eta(\boldsymbol{x}_i) > \eta]. \qquad (9)$$

The integral depends on the mean annual rate of all TCs for the place, the joint pdf $f_X(\boldsymbol{x})$, and the conditional probability $P[\eta(\boldsymbol{x}_i) > \eta]$ that a certain set of TC characteristics $\boldsymbol{x}_i$ will generate a water-level height greater than η. The annual occurrence rate of 1% is referred to as the hundred-year annual exceedance level, also known as the hundred-year return period.
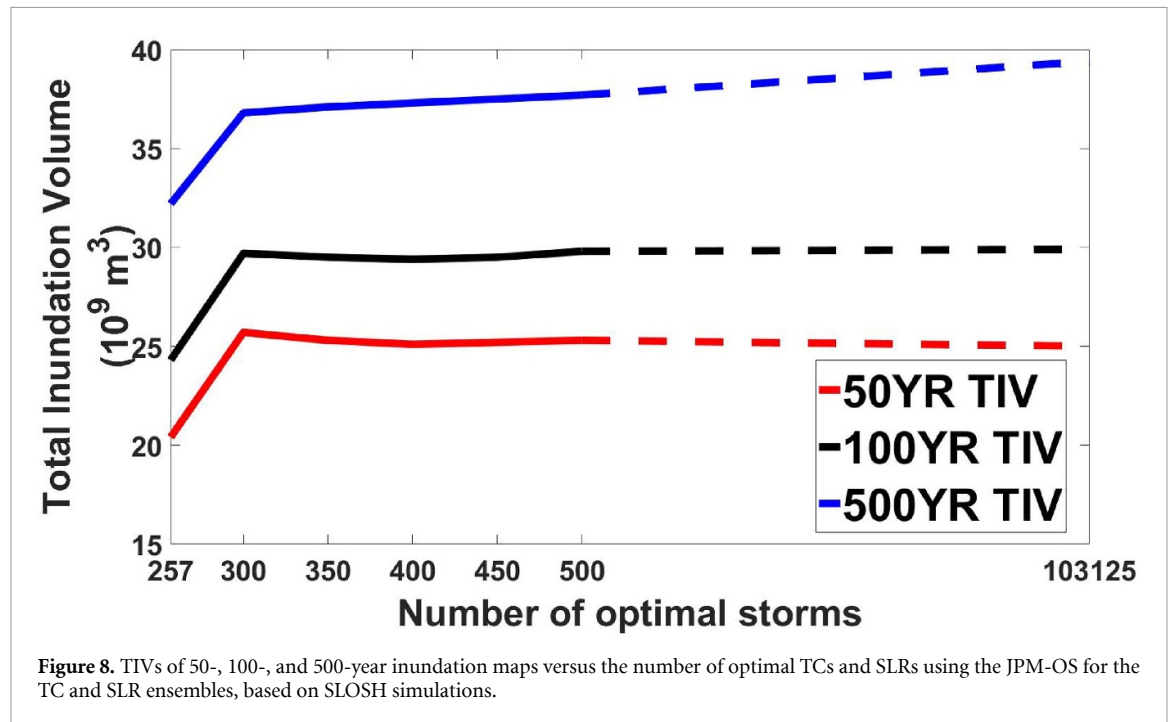
To calculate the probabilistic inundation maps using the JPM, five representative values are selected for each of P_c, R_m, θ, V_f, and SLR, and 33 representative values are selected for L_0. The ensemble contains a total of 103 125 storms (the test storm ensemble), and includes all the possible combinations of the discretized parameters. The representative values and corresponding probabilities for the parameters other than the landfall locations are shown in table 2. The probabilities of the landfall locations are shown in figure 6(e). The probabilities of SLR are calculated from the PDF of the GMSL shown in figure 7.

4.4.2. Joint probability method with optimal sampling for the TC and SLR ensemble
The JPM-OS selects several so-called optimal TC and SLR combinations from the test TC and SLR ensemble in table 2. The optimal TCs and SLRs are simulated using a coastal surge-wave model to obtain the storm surge responses, which are interpolated from the storm surge responses of the test TC and SLR ensemble. Probabilistic inundation maps are then calculated using equation (9). The highly accurate and efficient kriging surrogate model [23] is used as an interpolation scheme to estimate the water level of a TC and SLR based on the spatial covariance value and the water levels of the optimal TCs and SLRs.

Table 2. Representative values of the landfall TC parameters, the SLR, and the corresponding probabilities (in parentheses).

P_c (mb)	R_m (mile)	θ (deg.)	V_f (mph)	L_0 (n mi)	SLR (m)
25 (26.5%)	25 (16.1%)	0 (6.9%)	8 (19.7%)	−160–160	0.4 (14.4%)
45 (31.3%)	39 (25.9%)	16 (10.9%)	15 (31.2%)	Relative to CREF	0.7 (43.2%)
65 (24.8%)	53 (29.3%)	32 (23.8%)	22 (28.3%)	For every 10 nm	1.0 (25.6%)
85 (12.4%)	67 (19.7%)	48 (35.6%)	29 (15.1%)	—	1.4 (9.2%)
105 (5.0%)	81 (9.0%)	64 (22.8%)	36 (5.7%)	(33 locations)	1.8 (6.6%)

Figure 8. TIVs of 50-, 100-, and 500-year inundation maps versus the number of optimal TCs and SLRs using the JPM-OS for the TC and SLR ensembles, based on SLOSH simulations.

The number of optimal storms is determined by a regression plot showing the TIV of the inundation maps versus the number of optimal storms in figure 8. Three hundred and fifty optimal TCs and SLRs were selected from the test TCs and SLRs. As mentioned earlier, SLOSH was used for the selection of optimal TCs and SLRs to reduce the computational effort. This was found to be a robust procedure by Yang *et al* [24].

5. Summary

Probabilistic coastal inundation maps over large coastal flood plains for future climate are urgently needed for coastal adaptation and resilience planning by local coastal communities. Here, we present a novel method that considers the 6P joint PDFs of five TC characteristics and SLR in a large coastal flood plain in SWFL. When the 5P JPM-OS is used, the 1% annual chance of coastal inundation must be determined by conducting numerous sets of surge-wave simulations with the future TC ensemble, each for a different SLR scenario. With the 6P JPM-OS, however, the 1% coastal inundation risk can be determined using the future TC and SLR ensemble by conducting only one

set of surge-wave simulations, without having to subjectively choose a specific SLR scenario. In addition, the new 6P JPM and JPM-OS are much less uncertain and much more efficient than the traditional 5P JPM and JPM-OS.

Using TCs predicted by the FSUGSM-WRF models for 1982–2009, the 1% annual chance coastal inundation map was found to be comparable to those predicted by the historical TCs [23], and the 1% water level at the Naples tide gauge was found to agree well with that determined by the POT method using historical water-level data. According to TCs predicted by FSUGSM-WRF for 2080–2100 under the RCP8.5 scenario, the probabilistic coastal inundation will increase substantially. The TIV, TIA, AIH, and MIH will increase dramatically to (5.7, 2.4, 2.6, and 2.5) times their corresponding values in 1982–2009. These alarmingly large overland inundation predictions can inform coastal communities of realistic coastal inundation hazards and enable them to conduct urgently needed adaptation and resilience planning activities, and are much more useful than open-coast maximum surge and wave information [11, 12].

SLR plays a dominant role at the inland boundary. Near the coast, storm surge accounts for 70%–80% of the total inundation (for a 1 m SLR) or 30%–70%

(for a 2 m SLR). Therefore, TCs cannot be ignored in the development of future coastal flood maps. The effect of SLR on inundation varies significantly over the floodplain, due to the nonlinear interaction between storm surge and the SLR. SLR-induced coastal inundation can be amplified or reduced by the surge–SLR interaction, depending on location. Hence, coastal flood maps produced using a 'bathtub' model, which adds the SLR value uniformly throughout the floodplain or onto a flood map, are inaccurate.

The new 6P JPM-OS, which offers less uncertainty and more efficiency, can be used to produce reliable probabilistic coastal inundation for large coastal flood plains quickly. This method can be extended to include additional parameters such as precipitation and soil moisture content if they are known. The method presented here can readily be applied to TCs predicted by other climate and downscaling models. To further reduce the uncertainty in predicting future coastal inundations, a comprehensive study of the sensitivity of future TCs and SLR to numerous climate models and downscaling models is recommended.

Data availability statement

The data that support the findings of this study are available upon reasonable request from the authors.

Acknowledgments

ORCID iD

Y Peter Sheng ⬤ https://orcid.org/0000-0001-8827-1451

References

[1] Kopp R E, Horton R M, Little C M, Mitrovica J X, Oppenheimer M, Rasmussen D J, Strauss B H and Tebaldi C 2014 Probabilistic 21st and 22nd century sea-level projections at a global network of tide-gauge sites *Earth's Future* **2** 383–406

[2] Sweet W V, Kopp R E, Weaver C P, Obeysekera J, Horton R M, Thieler E R and Zervas C 2017 Global and regional seal level rise scenarios for the United States *NOAA Technical Report NOA CO-OPS* 083 (NOAA/NOS Center for Operational Oceanographic Products and Services)

[3] Horton B P, Kopp R E, Garner A J, Hay C C, Khan N S, Roy K and Shaw T A 2018 Mapping sea-level change in time, space, and probability *Annu. Rev. Environ. Resour.* **43** 481–521

[4] Knutson T, McBride J, Chan J, Emanuel K, Holland G, Landsea C, Held I, Kossin J, Srivastava A and Sugi M 2010 Tropical cyclones and climate change *Nat. Geosci.* **3** 157–63

[5] Villarini G and Vecchi G A 2013 Projected increases in North Atlantic tropical cyclone intensity from CMIP5 models *J. Clim.* **26** 3231–40

[6] Knutson T *et al* 2020 Tropical cyclones and climate change assessment: part II: projected response to anthropogenic warming *Bull. Am. Meteorol. Soc.* **101** E303–22

[7] Emanuel K 2021 Response of global tropical cyclone activity to increasing CO_2: results from downscaling CMIP6 models *J. Clim.* **34** 57–70

[8] Sheng Y P, Rivera-Nieves A, Zou R and Paramygin A 2021 Role of wetlands in reducing structural loss is highly dependent on characteristics of storms and local wetland and structure conditions *Sci. Rep.* **11** 5237

[9] National Research Council 2009 *Mapping the Zone: Improving Flood Map Accuracy* (Washington, DC: The National Academies Press)

[10] Lin N, Emanuel K, Oppenheimer M and Vanmarcke E 2012 Physically based assessment of hurricane surge threat under climate change *Nat. Clim. Change* **2** 462–7

[11] Nadal-Caraballo N C and Melby J A 2015 North Atlantic Coast comprehensive study phase I: statistical analysis of historical extreme water levels with sea level change *J. Coast. Res.* **32** 35–45

[12] Marsooli R and Lin N 2018 Numerical modeling of historical storm tides and waves and their interactions along the US East and Gulf Coasts *J. Geophys. Res.* **123** 3844–74

[13] Marsooli R and Lin N 2020 Impacts of climate change on hurricane flood hazards in Jamaica Bay, New York *Clim. Change* **163** 2153–71

[14] Wu S, Feng A, Gao J, Chen M, Li Y and Wang L 2017 Shortening the recurrence periods of extreme water levels under future sea-level rise *Stoch. Environ. Res. Risk Assess.* **31** 2573–84

[15] Tebaldi C, Strauss B H and Zervas C E 2012 Modelling sea level rise impacts on storm surges along US coasts *Environ. Res. Lett.* **7** 014032

[16] Condon A J and Sheng Y P 2012 Evaluation of coastal inundation hazard for present and future climates *Nat. Hazards* **62** 345–73

[17] LaRow T E, Lim Y-K, Shin D W, Chassignet E P and Cocke S 2008 Atlantic basin seasonal hurricane simulations *J. Clim.* **21** 3191–206

[18] LaRow T E, Stefanova L and Seitz C 2014 Dynamical simulations of North Atlantic tropical cyclone activity using observed low frequency SST oscillation imposed on CMIP5 model RCP4.5 SST projections *J. Clim.* **27** 8055–69

[19] Chylek P, Li J, Dubey M K, Wang M and Lesins G 2011 Observed and model simulated 20th century Arctic temperature variability: Canadian earth system model CanESM2 *Atmos. Chem. Phys. Discuss.* **11** 22893–907

[20] Moss R H, Nakicenovic N and O'Neil B C 2008 *Towards New Scenarios for Analysis of Emissions, Climate Change, Impacts, and Response Strategies* (Geneva: IPCC)

[21] Moss R H *et al* 2010 The next generation of scenarios for climate change research and assessment *Nature* **463** 747–56

[22] Liu B, Costa K, Xie L and Semazzi F 2014 Dynamical downscaling of climate change impacts on wind energy resources in the contiguous United States by using a limited-area model with scale-selective data assimilation *Adv. Meteorol.* **2014** 1–11

[23] Yang K, Paramygin V and Sheng Y P 2019 An objective and efficient method for estimating probabilistic coastal inundation hazards *Nat. Hazards* **99** 1105–30

[24] Kopp R E, Gilmore E A, Little C M, Lorenzo-Trueba J, Ramenzoni V C and Sweet W V 2019 Usable science

for managing the risks of sea-level rise *Earth's Future* **7** 1235–69

[25] Jevrejeva S, Grinsted A and Moore J C 2014 Upper limit for sea level projection by 2100 *Environ. Res. Lett* **9** 104008

[26] Sheng Y P *et al* 2012 A regional testbed for storm surge and coastal inundation models—an overview *Proc. Int. Conf. on Estuarine and Coastal Modeling (St. Augustine, FL, 7–9 November 2011)* (Spaulding: American Society of Civil Engineers) pp 476–95

[27] Sheng Y P 1987 On modeling three-parameter estuarine and marine hydrodynamics *Three-Parameter Models of Marine and Estuarine Dynamics* ed J C J Nihoul and B M Jamart (Amsterdam: Elsevier Science Publishing Company) pp 35–54

[28] Sheng Y P 1990 Evolution of a three-parameter curvilinear-grid hydrodynamic model for estuaries, lakes and coastal waters: CH_3D *Estuarine and Coastal Modeling: Proc. Estuarine and Coastal Circulation and Pollutant Transport Model Data Comparison Specialty Conf.* (Reston, VA: ASCE) pp 40–49

[29] Sheng Y P, Zhang Y and Paramygin V A 2010 Simulation of storm surge, wave, and coastal inundation in the Northeastern Gulf of Mexico region during Hurricane Ivan in 2004 *Ocean Modelling* **35** 314–31

[30] Sheng Y P, Alymov V and Paramygin V A 2010 Simulation of storm surge, wave, currents, and inundation in the Outer Banks and Chesapeake Bay during Hurricane Isabel in 2003: the importance of waves *J. Geophys. Res.* **115** 1–27

[31] Booij N, Ris R C and Holthuijsen L H 1999 A third-generation wave model for coastal regions: model description and validation *J. Geophys. Res.* **104** 7649–66

[32] Bilskie M V, Hagen S C, Alizad K, Medeiros S C, Passeri D L, Needham H F and Cox A 2016 Dynamic simulation and numerical analysis of hurricane storm surge under sea level rise with geomorphologic changes along the northern Gulf of Mexico *Earth's Future* **4** 177–93

[33] Wang T and Yang Z 2019 The nonlinear response of storm surge to sea-level rise: a modeling approach *J. Coast. Res.* **35** 287–94

[34] Miller K G, Kopp R E, Horton B P, Browning J V and Kemp A C 2013 A geological perspective on sea-level rise and its impacts along the US mid-Atlantic coast *Earth's Future* **1** 3–18

[35] Sheng Y P, Lapetina A and Ma G 2012 The reduction of storm surge by vegetation canopies: three-parameter simulations *Geophys. Res. Lett.* **39** 1–5

[36] Sheng Y P and Zou R 2017 Assessing the role of mangrove forest in reducing coastal inundation during major hurricanes *Hydrobiologia* **803** 87–103

[37] Yang K, Paramygin V A and Sheng Y P 2020 A rapid forecasting and mapping system of storm surge and coastal flooding *Wea Forecast.* **35** 1663–81

[38] Taylor K, Stouffer R and Meehl G 2012 An overview of CMIP5 and the experiment design *Bull. Am. Meteorol. Soc.* **93** 485–98

[39] Hall T M, Kossin J P, Thompson T and McMahon J 2021 US tropical cyclone activity in the 2030s based on projected changes in tropical sea surface temperature *J. Clim.* **34** 1321–35

[40] Knutson T, Sirutis J, Garner S, Vecchi G A and Held I M 2008 Simulated reduction in Atlantic hurricane frequency under twenty-first-century warming conditions *Nat. Geosci.* **1** 359–64

[41] Resio D T, Asher T G and Irish J L 2017 The effects of natural structure on estimated tropical cyclone surge extremes *Nat. Hazards* **88** 1609–37

[42] Lin N, Kopp R E, Horton B P and Donnelly J P 2016 Sandy's flood frequency from 1800 to 2100 *Proc. Natl Acad. Sci.* **113** 12071–5

[43] Eyring V, Bony S, Meehl G A, Senior C A, Stevens B, Stouffer R J and Taylor K E 2016 Overview of the coupled model intercomparison project phase 6 (CMIP6) experimental design and organization *Geosci. Model Dev.* **9** 1937–58

[44] Jelesnianski C P, Chen J and Shaffer W A 1992 SLOSH: sea, lake, and overland surges from hurricanes *NOAA Tech. Rep. NWS* 48 (Silver Spring, MD: US Department of Commerce, National Oceanic and Atmospheric Administration, National Weather Service)

[45] Skamarock W C, Klemp J B, Dudhia J, Gill D O, Baker D M, Duda M G, Huang X Y, Wang W and Powers J G A 2018 Description of the advanced research WRF version 3 *NCAR Tech, Note NCAR/TN-475+STR* p 113

[46] Chouinard L E and Liu C 1997 A model for the severity of hurricanes in the Gulf of Mexico *J. Waterway Port Coast. Ocean Eng.* **123** 113–9